



# Visible light–driven ZnO/Fe<sub>3</sub>O<sub>4</sub> magnetic nanoparticles for detoxification of diazinon: the photocatalytic optimization process with RSM-BBD model

Sima Kalantar<sup>1</sup> · Akram Bemani<sup>1</sup> · Mohammad Hossein Sayadi<sup>2,3</sup> · Elham Chamanehpour<sup>2</sup>

Received: 27 March 2023 / Accepted: 24 July 2023 / Published online: 9 August 2023  
© The Author(s), under exclusive licence to Springer-Verlag GmbH Germany, part of Springer Nature 2023

## Abstract

Today, diazinon is one of the most widely used organophosphorus pesticides, whose widespread use can cause many ecological and biological risks. In this research, a magnetic ZnO/Fe<sub>3</sub>O<sub>4</sub> nanoparticle was used to investigate the photocatalytic degradation of diazinon. Sol-gel synthesis was used to create the nanoparticle, which was then characterized using XRD, FTIR, FESEM, VSM, and XPS techniques. The design of photocatalytic degradation experiments was done using the response surface method and the Box-Behnken design model. The investigated parameters include pH, nanoparticle concentration, diazinon concentration, and irradiation time. The characterization of the ZnO/Fe<sub>3</sub>O<sub>4</sub> nanoparticle showed well-formed crystalline phases and a cubic spinel structure. Additionally, the shape of the nanoparticle is almost uniform and spherical. The FT-IR spectrum also confirmed the presence of all functional groups related to ZnO and Fe<sub>3</sub>O<sub>4</sub> in the ZnO/Fe<sub>3</sub>O<sub>4</sub> nanoparticles structure. The synthesized nanocomposite has superparamagnetic properties and a very small coercive field, making it easily recyclable, according to a VSM analysis. XPS results also showed the presence of Fe (Fe 2p<sub>1/2</sub> and Fe 2p<sub>3/2</sub>), Zn (Zn 2p<sub>1/2</sub> and Zn 2p<sub>3/2</sub>), oxygen (O1s), and weak carbon (C1s) peaks in the ZnO/Fe<sub>3</sub>O<sub>4</sub> structure. The results of the photocatalytic optimization experiments showed that the highest efficiency of diazinon toxin degradation is 99.3% under the conditions of pH 7, diazinon initial concentration of 10 mg/L, nanoparticle concentration of 1 g/L, and a contact time of 90 min. This result is very close to the BBD model's predicted removal efficiency under optimal conditions (100%). As a result, the ZnO/Fe<sub>3</sub>O<sub>4</sub> nanocomposite can produce active free radicals through UV radiation, and these radicals can successfully remove diazinon under actual conditions.

**Keywords** Photocatalysis reduction · Organophosphorus poison · Response surface methodology · Recyclable · Degradation mechanism

## Highlights

- A heterogeneous photocatalyst, ZnO/Fe<sub>3</sub>O<sub>4</sub>, was synthesized as a highly active, easily separable, and recyclable catalyst for the oxidative degradation of diazinon toxin in an aqueous solution.
- A Box–Behnken design model was used to optimize experimental conditions.
- Under optimized conditions, the degradation of diazinon was obtained 99.3%.
- ZnO/Fe<sub>3</sub>O<sub>4</sub> was an effective and performable integrated system into efficient degradation of toxic organics.

Responsible Editor: Sami Rtimi

✉ Akram Bemani  
a.bemani@ardakan.ac.ir

Extended author information available on the last page of the article

## Introduction

Today, organic pollutants are among the most important and dangerous pollutants in water resources. Due to the release of hazardous and cancer-causing substances in the aqueous phase, the presence of these contaminants has caused serious health and environmental problems (Liang et al., 2021). In the meantime, pesticides are one of the most common organic pollutants that are being considered today. Under normal environmental conditions, the majority of pesticides' active substances are resistant. Surface and subsurface water contamination is a result of pesticides' persistence in aquatic environments and their potential undesirable health effects. There is a lot of concern now about the possible adverse effects of these

pesticides' presence in food and water on human health and ecosystem balance (Zadeh et al., 2021). Among the possible chronic effects of these compounds, we can mention carcinogenesis, neurological disorders, effects on reproduction, and effects on cell growth, especially in the early stages of life. In addition, typical oxidation processes might result in the formation of mutagenic compounds (Farmany et al., 2016).

Meanwhile, organophosphorus pesticides are one of the most widely used pesticides in the world, which enter water sources in various ways, including industrial effluents, agricultural runoff, and the use of chemicals (Toolabi et al., 2018). They also have the highest consumption of all pesticides and are widely used in agriculture to increase production and resolve nutritional needs (Sillanpää et al., 2018). Diazinon is one of the most well-known phosphorus-containing pesticides and has been classified by the World Health Organization as a class II dangerous substance (Salarian et al., 2016). Diazinon is non-polar and relatively soluble in water. Also, it is mobile and stable in soil and does not evaporate easily from soil or water. Therefore, its presence in drinking water and groundwater seems to be of concern (Kalantary et al., 2015). The oral toxicity of this insecticide is around 300 mg/kg. This pesticide's acute toxicity can cause diseases like cancer, nervous system disorders, severe intestinal contractions, and low blood pressure (Dehghani et al., 2019) (Fig. 1).

So far, processes such as surface absorption, filtration, membrane separation, biological decomposition, and chemical coagulation have been used to remove diazinon (Ghodsii et al., 2020). Because they just transport pollutants from one phase to another and only partially remove them, these methods are not very effective for purification. They can also generate secondary toxic contaminants and are not cost-effective (Sayadi et al., 2022a). Advanced oxidation techniques (AOPs) have recently been introduced as efficient methods for removing diazinon. One of the most effective AOPs for oxidizing resistant organic materials and changing

their nature is photocatalytic oxidation (Yang et al., 2021). Through this process, pollutants are broken down by UV irradiation. Radiation stimulates the semiconductor catalyst, which leads to electron transfer to the molecule's surface layers and the production of electron-holes. The resulting hole has a strong oxidizing and electron-reviving property, and with the production of hydroxyl radicals, it causes the degradation of polluting organic molecules (Chamanehpour et al., 2022). Today, photocatalytic processes using nanoparticles are very efficient methods that result in the complete mineralization and degradation of organic pollutants without the production of harmful compounds in the environment (Ghodsii et al., 2020).

Among the different types of semiconductor photocatalysts, zinc oxide nanoparticles can be recognized as a practical photocatalyst for diazinon removal due to their environmental friendliness, electrochemical and electrical properties (Abebe et al., 2021), high light absorption coefficient, cheapness, fast electron-hole transfer, and chemical stability (Ghaderi et al., 2018). But, because of its wide bandgap (3.37 eV), light can only be absorbed in the UV region. Also, pure ZnO is inherently an insulator, which restricts its application in electrical and optoelectronic devices that need conducting or semiconducting components (Wang et al., 2021). The formation of a nanoparticle via n-n or n-p junctions and fostering heterogeneous bonding with the addition of metal oxides and photosensitizers to ZnO can enhance its photodegradation (Abebe et al., 2020a). These metal oxides can have several functions, which include the following: (1) changing the band gap can increase the amount and range of light absorption. (2) By combining two metal oxides, rough surfaces can increase porosity, and thus facilitate electron transfer (Goyal et al., 2018). (3) A higher degree of porosity improves the absorption of diazinon by the formed nanoparticle (Długosz et al. 2021). (4) ZnO nanoparticle modification can provide multipurpose products with unique properties in addition to enhancing the photocatalyst's properties (Sin et al., 2018). (5) The construction of heterogeneous bonds adjusts the transport of electrons.

Among metal oxides, Fe<sub>3</sub>O<sub>4</sub> nanoparticles have a high photocatalytic activity, a simple operation, a synergistic effect with other nanoparticles, and have magnetic properties (Wang et al., 2016). This magnetic feature makes it easier to recycle the nanoparticle, and after photodegradation, a strong external magnetic field can easily separate the nanoparticle (Długosz et al. 2021). These nanoparticles have been highly regarded for the creation of metal composites because of their accessibility, affordability, friendliness to the environment, and thermodynamic stability (Abebe et al., 2020b). Many studies have been conducted on the removal of pollutants with nanomaterials, such as the 100% removal of atrazine pesticide by using Fe<sub>3</sub>O<sub>4</sub>-TiO<sub>2</sub>/rGO (Boruah and Das, 2020), the decomposition of 85.2%

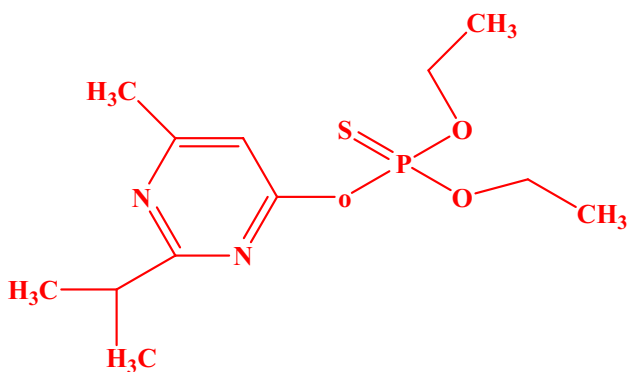


Fig. 1 Molecular structure of diazinon

of diazinon toxin under optimal conditions using graphene/ZnO doped with manganese under ultraviolet light (Mohammadi et al., 2019), and the 85% removal of diazinon by sonophotocatalytic process using TiO<sub>2</sub> nanoparticles doped with iron (Tabasideh et al., 2017).

On the other hand, it is crucial to pay attention to the design of experiments for reasons including maximizing the validity of results, efficient use of resources, repeatability, optimization, improving processes, and saving time and money. Response surface methodology (RSM) is one of the test design methods that are used to optimize the effective parameters of the test. RSM is a mathematical and statistical technique used to model and optimize complex interactions between several variables and an interest response (Singh and Verma, 2019). N-doped TiO<sub>2</sub> nanosheets were utilized by Salarian et al. in the RSM method to remove diazinon. They used central composite design (CCD) to model and improve operational degradation factors such as pH, catalyst dose, initial pollutant concentration, and irradiation time. Their results showed that the modeling can determine the optimal parameters well and predict the acceptable amount of degradation (Salarian et al., 2016).

In this regard, the goal of this research is to investigate the efficacy of ZnO/Fe<sub>3</sub>O<sub>4</sub> magnetic nanocomposite for photocatalytic removal of the diazinon toxin from aqueous environments. This research has tried to achieve a comprehensive and systematic method for the removal of pollutants by combining modeling methods, experimental tests, and software analysis in order to achieve high performance in photocatalytic degradation with the least number of test runs. To improve the performance of the synthesis nanoparticle in removing the diazinon pollutant, parameters such as solution pH, contact time, nanoparticle concentration, and toxin concentration were also optimized using the response surface method. Due to the high amount of hydroxyl radical produced, easy access, non-toxicity, production of electron-hole pairs, and decreased recombination rate, the synthesized nanoparticle is capable of high photocatalytic activity, which is more than ZnO and Fe<sub>3</sub>O<sub>4</sub>. In addition, it has a great capacity to remove organic contaminants, especially diazinon toxin, by generating active oxidative species like OH•.

## Material and method

### Raw materials

Zinc nitrate 99.9% (Zn(NO<sub>3</sub>)<sub>2</sub>), iron (II) sulfate heptahydrate 99% (FeSO<sub>4</sub>·7H<sub>2</sub>O), sodium hydroxide 98% (NaOH),

tetraethyl orthosilicate 99.9% (SiC<sub>8</sub>H<sub>20</sub>O<sub>4</sub>), and ethanol 99% (C<sub>2</sub>H<sub>6</sub>O) were purchased from Sigma Aldrich and Merck.

### Synthesis of ZnO/Fe<sub>3</sub>O<sub>4</sub> nanoparticles

At first, zinc oxide nanoparticles were synthesized using the co-precipitation method. A solution of 0.5 M Zn(NO<sub>3</sub>)<sub>2</sub> was prepared in 50 ml of distilled water. Using a 1 M NaOH solution, the pH value was adjusted to 8. The solution was kept at 80 °C for 5 h. The sediment was collected, washed, and dried. Finally, it was calcined at 400 °C for 1 h. The resulting white precipitate shows ZnO nanoparticles (Elshypany et al., 2021). Then, using an oxidation method, Fe<sub>3</sub>O<sub>4</sub> nanoparticles were synthesized. First, 100 ml of distilled water was used to dissolve 0.027 g of FeSO<sub>4</sub>·7H<sub>2</sub>O. By adding a dropwise 6 M NaOH solution to the previous solution, the pH is adjusted to 11. Air flow was then introduced, and the solution was kept at 25 °C for an additional hour. The precipitate of Fe<sub>3</sub>O<sub>4</sub> was washed and dried in an oven (Sayadi et al., 2019). ZnO/Fe<sub>3</sub>O<sub>4</sub> magnetic nanocomposite was created using the sol-gel method. By using ultrasonic, an appropriate amount of Fe<sub>3</sub>O<sub>4</sub> and ZnO with a weight ratio of 0.8:1 was dispersed separately in a mixture of ethanol and water (1:4). In a separate container, 1 ml of tetraethyl orthosilicate (TEOS) was added to the solvent solution, and 2 ml of 0.1 normal HCl was added to it under stirring conditions. Then, the solution containing ZnO nanoparticles was added to the TEOS solution, and after 15 min, the solution containing Fe<sub>3</sub>O<sub>4</sub> nanoparticles was also added to the above solution under mechanical stirring. To form a gel, the solution was stirred for an additional 6 h. The resultant gel was vacuum-dried at 60 °C for 2 h to produce the powder. The resulting deposit is ZnO/Fe<sub>3</sub>O<sub>4</sub> nanoparticles (Wong et al., 2011).

### Characterization

To identify and determine the properties of the produced nanoparticles, numerous analyses are needed. X-ray diffraction (Rigaku Ultima IV XRD) and Cu Kα radiation (λ = 0.15418 nm) were used to determine the samples' crystal structure and crystalline phase. Additionally, a field emission scanning electron microscope was used to determine the morphology and size of the synthesized nanoparticles (FESEM, ZEISS Sigma 300). XPS analysis (VG ESCALAB 210 electron spectrometer) was used to identify the existing compounds and chemical states of the desired nanoparticles. A VSM device (LBKFB, Iran) was also used to check the sample's magnetic characteristics. FT-IR analysis (Thermo Nicolet Avatar 360) was used to identify the compounds and bonds in the desired nanoparticles.

## Optimization of parameters

The Design-Expert 7.0.0 software's Box-Behnken Design (BBD) model was used to carry out the optimization process. BBD is one of the design models in the response surface method (RSM). BBD makes it easier to optimize the useful parameters with the minimum number of experiments and also provides the possibility of analyzing the interaction between the parameters (Polat & Sayan, 2019). The investigated variables include pH, contact time, amount of nanoparticles, and diazinon concentration. To investigate the effects of parameters, 30 test runs over 2 days were selected. Diazinon concentrations of 10 to 50 mg/L, solution pH of 3 to 11, contact times of 10 to 120 minutes, and catalyst concentrations of 0.1 to 1 g/L were defined in the model. Each sample's pH was adjusted using either 1 M HCl or 1 M NaOH.

## Photocatalytic removal of diazinon

The photocatalytic removal experiments on diazinon were carried out in a 100-ml Pyrex reactor under UV-C light (6 W, Philips, 254 nm spectrum) at ambient temperature and pressure after determining the values of the parameters in each experimental run. The pH settings, contact time, amount of nanoparticles, and diazinon concentration were all known for each test run. After the completion of each run, a sample of the solution was taken in order to use a spectrophotometer to measure the concentration of diazinon at a wavelength of 247 nm. Using reaction (1), determine the volume of diazinon removal by photocatalytic degradation (Ahmadpour et al., 2020):

$$\text{Diazinon Removal}(\%) = \frac{C_0 - C_e}{C_0} \times 100 \quad (1)$$

In this relationship,  $R$  is the pollutant decomposition efficiency (percent),  $C_0$  is the initial concentration of the pollutant in the solution (mg/l), and  $C_e$  is the final concentration of the pollutant in the solution after the decomposition process (mg/l).

Finally, the optimal value of each experimental parameter was determined, and the experiment was repeated once again under optimal conditions to determine the amount of diazinon photocatalytic removal under optimal conditions. Additionally, after each test under ideal conditions, the produced nanoparticles were collected using a magnet and cleaned many times with distilled water to assess its capacity to be reused. It was then dried for 2 h at 60 °C.

The resulting precipitate was used in five test cycles to measure the reusability of the nanoparticles to remove diazinon (Chamanehpour et al., 2022).

## Results

### Characterization of ZnO/Fe<sub>3</sub>O<sub>4</sub> nanoparticles

The synthesized nanoparticle structural characteristics were analyzed and investigated by XRD, FT-IR, FESEM, XPS, and VSM analyses. These results are described below.

#### XRD spectrum

The X-ray diffraction pattern of ZnO/Fe<sub>3</sub>O<sub>4</sub> nanoparticles is presented in Fig. 2a. As can be observed in the figure, the existence of diffraction peaks for ZnO/Fe<sub>3</sub>O<sub>4</sub> demonstrates the formation of crystalline phases and the cubic spinel structure of the nanoparticles. The drawn pattern matches JCPDS standard patterns No. 36-1451 for ZnO (Chu et al., 2021) and No. 19-0629 for Fe<sub>3</sub>O<sub>4</sub> (Sayadi et al., 2022b).  $2\theta$  equals 30.81°, 34.44°, 35.58°, 47.60°, 56.62°, 57.18°, 62.63°, and 67.97° belong to the crystal planes (100), (002), (311), (102), (110), (511), (440), and (112) respectively. These peaks relate to the hexagonal phase of ZnO and the cubic spinel phase of Fe<sub>3</sub>O<sub>4</sub>, which are shown in the figure with red and blue colors, respectively (Erim et al., 2022; Sajjadi et al., 2019). The Debye–Scherrer reaction (Reaction 2) was used to determine the average crystallographic size of the particles using the XRD results (Chamanehpour et al., 2023):

$$D = \frac{k\lambda}{\beta \cos\theta} \quad (2)$$

where  $\beta$  is the width of the peak at half maximum intensity in radians (FWHM),  $\theta$  is the angle of the peak location,  $D$  is the crystal size of the particles, and  $\lambda$  is the wavelength of the X-ray corresponding to KUK $\alpha$  (0.154056 nm), and the coefficient  $k$  for spherical particles is 0.9. According to the preferred peak (the peak with the highest intensity), the average crystal size of the particles for the ZnO/Fe<sub>3</sub>O<sub>4</sub> nanoparticles sample was found to be about 45 nm.

#### FT-IR spectrum

Figure 2 b displays the ZnO/Fe<sub>3</sub>O<sub>4</sub> nanoparticles FT-IR spectra in the 400–4000 cm<sup>-1</sup> regions. The resulting inverse absorption peaks in this spectrum can be used to identify the bonds in the sample. A strong inverse absorption peak at around 3500 cm<sup>-1</sup> is visible in the FT-IR spectra of the ZnO/Fe<sub>3</sub>O<sub>4</sub> nanoparticles and is attributable to the vibrational stretching groups O–H and H–O–H found in the structure of the absorbed water molecules (Liu et al., 2015). Additionally, the surface absorption of water and hydroxyl groups is related to the strong inverse absorption peak at

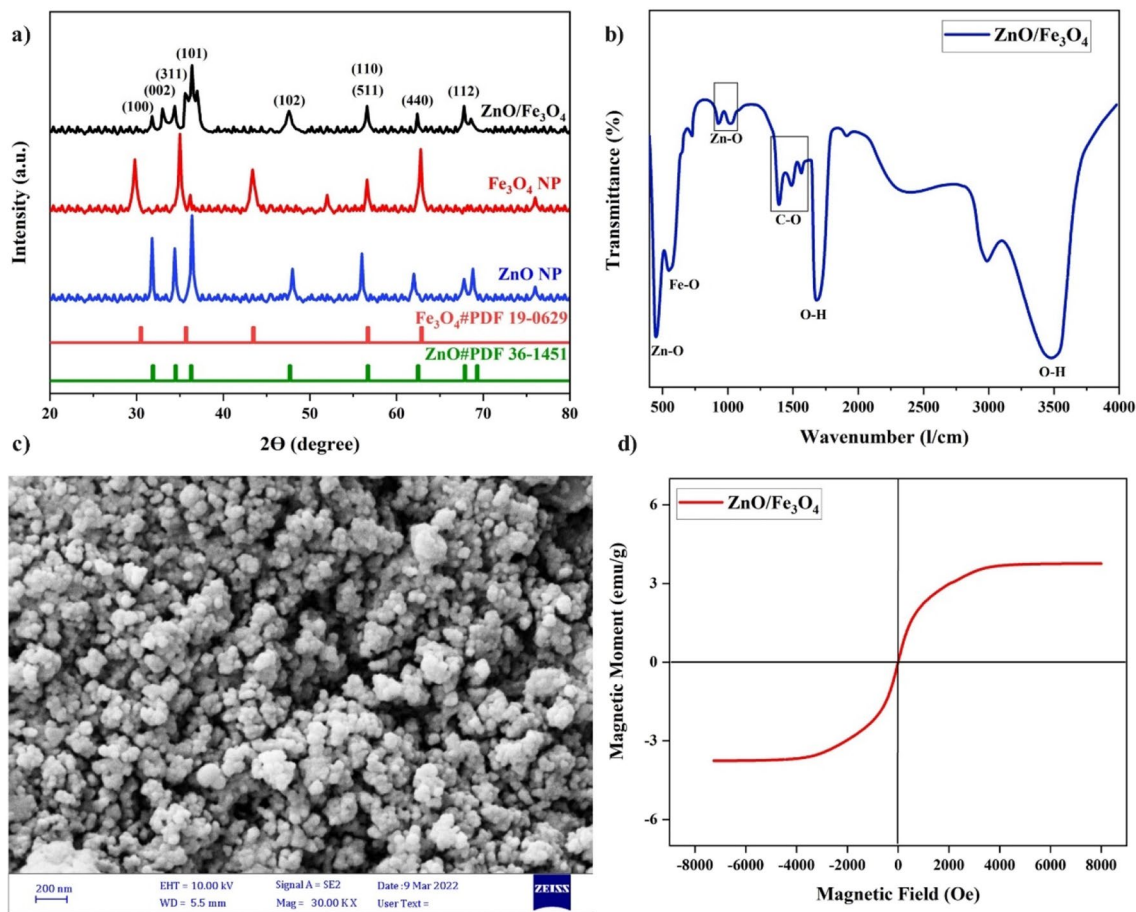


**Fig. 2** Characterization of ZnO/Fe<sub>3</sub>O<sub>4</sub> nanoparticles (**a** XRD, **b** FTIR, **c** FESEM, **d** VSM)

1700 cm<sup>-1</sup> (Mahmoodabadi et al., 2018). Inverse absorption peaks located between 900 and 1700 cm<sup>-1</sup> are attributed to C–O groups (Durmus et al., 2015; Zhang and Wu, 2013). The inverse absorption peaks located at about 400 and 600 cm<sup>-1</sup> seen in the ZnO/Fe<sub>3</sub>O<sub>4</sub> nanoparticles are respectively related to the Fe–O and Zn–O metal-oxygen groups present in the structure of the nanoparticles (Chireh et al., 2019; Goyal et al., 2015). The results showed that all functional groups related to ZnO and Fe<sub>3</sub>O<sub>4</sub> are present in the synthesized ZnO/Fe<sub>3</sub>O<sub>4</sub> nanoparticle structure, which can play a key role in pollutant absorption.

#### FESEM analysis

By using FESEM images, the morphology of the ZnO/Fe<sub>3</sub>O<sub>4</sub> nanoparticles was investigated. As seen in Fig. 2c, the nanoparticles have an almost spherical and uniform shape, and some particles are stuck together, which is inevitable due to the inherent magnetic property of iron ferrite (Fe<sub>3</sub>O<sub>4</sub>) particles. The accumulation of particles might also be caused by the temperature rise that occurs during heat treatment. In other words, some degree of particle

accumulation at high temperatures is inevitable as a result of the fusion of a variety of neighbors caused by the melting of the particle's surface (Wu et al., 2015; Naseri et al., 2016). Using the software Digimizer, the average particle size was determined to be 41 nm, which is consistent with previous studies (Bisht et al., 2016).

#### VSM analysis

The vibrating sample magnetometer curve of the ZnO/Fe<sub>3</sub>O<sub>4</sub> nanoparticles sample is shown in Fig. 2d. According to its shape, the sample exhibits superparamagnetic behavior with a very small coercive field and has a very small hysteresis loop (Habibi-Yangjeh and Golzad-Nonakaran, 2018). The saturation magnetization ( $M_s$ ) for ZnO/Fe<sub>3</sub>O<sub>4</sub> nanoparticles was obtained at 4 emu/g. Therefore, it can be claimed that the magnetic property of the combined catalyst of iron ferrite and zinc oxide makes it simple for a magnet to separate it from the aqueous solution. In practical applications of photocatalysts, catalyst stability and recycling play an important role, and the synthesized nanoparticles have this property.

**XPS spectrum**

With the use of X-ray photoelectron spectrometry, Fig. 3 shows the chemical state of the final ZnO/Fe<sub>3</sub>O<sub>4</sub> nanoparticle surface, which has been demonstrated separately in the general extent and also in the bond energy related to iron and zinc peaks. The results show the presence of Fe (Fe 2p<sub>1/2</sub>, Fe 2p<sub>3/2</sub>, and Fe 3p), Zn (Zn 2p<sub>1/2</sub>, Zn 2p<sub>3/2</sub>, Zn 3d, and Zn 3s), oxygen (O1s), and weak carbon (C1s) peaks. In high-resolution spectra, the binding energies of the Fe 2p<sub>1/2</sub>, Fe 2p<sub>3/2</sub>, Zn 2p<sub>1/2</sub>, and Zn 2p<sub>3/2</sub> peaks are 724.9, 711.3, 1044.9, and 1021.7 electron volts, respectively (Elshypany et al., 2021). The presence of Fe<sub>3</sub>O<sub>4</sub> and ZnO phases on the surface of the ZnO/Fe<sub>3</sub>O<sub>4</sub> nanoparticles is confirmed by the appearance of peaks associated with iron and zinc. Also, the presence of an oxygen peak at around 530 eV is another proof of the iron oxide and

zinc oxide phases’ formation (Dehghan et al., 2018; Erim et al., 2022).

**Optimization of parameters**

The parameters were optimized using the BBD design method. The proposed models, which have *p* values less than 0.05, are linear and quadratic (Table 1). The quadratic model was used for optimization because it also considered the interaction of parameters. The data fit this model at a significance level of 95%. The experiment was designed to take place over a period of 2 days and 30 test repetitions, the values of which are displayed in Table 2 for each test run. As can be observed, the BBD method’s predicted values and the actual values are quite similar.

To assess the adequacy of the quadratic model, ANOVA was used (Table 3). *p* values under 0.05 show that the

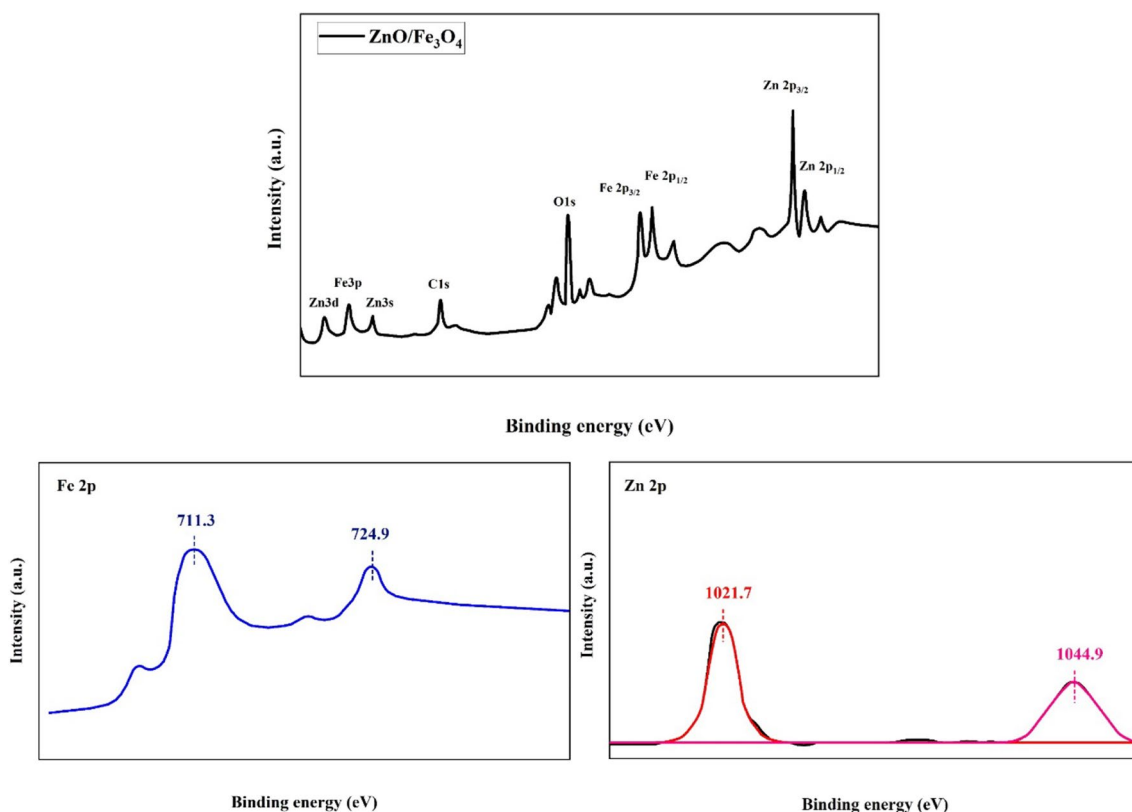


**Fig. 3** XPS spectrum of ZnO/Fe<sub>3</sub>O<sub>4</sub> nanoparticles and high-resolution spectrum related to iron and zinc

**Table 1** Proposed models in BBD design method

Source	Sequential <i>p</i> value	Lack of Fit <i>p</i> value	Adjusted <i>R</i> <sup>2</sup>	Predicted <i>R</i> <sup>2</sup>	situation
Linear	0.0018	0.0005	0.4154	0.2605	Suggested
2FI	0.9099	0.0003	0.2987	− 0.3262	–
Quadratic	0.0025	0.0016	0.7016	0.0284	Suggested
Cubic	0.0114	0.0141	0.9382	− 2.8621	Aliased

**Table 2** Runs of optimization experiments

Block	Run	pH	Time (min)	Catalyst dose (g/L)	Diazinon dose (mg/L)	Actual removal (%)	Predicted removal (%)
Day 1	1	3	10	0.1	50	50	48.69
Day 1	2	11	120	1	10	98	99.79
Day 1	3	3	120	1	10	95	88.69
Day 1	4	7	60	0.5	30	88	86.91
Day 1	5	11	10	1	50	62.8	58.36
Day 1	6	11	10	0.1	10	77	68.02
Day 1	7	11	10	0.1	50	55	58.89
Day 1	8	11	120	1	50	76	76.57
Day 1	9	3	120	0.1	10	63	68.83
Day 1	10	7	60	0.5	30	85	86.91
Day 1	11	3	10	0.1	10	64	61.99
Day 1	12	11	120	0.1	50	78.5	73.02
Day 1	13	3	120	0.1	50	55	52.38
Day 1	14	3	10	1	50	61	53.53
Day 1	15	7	60	0.5	30	87.3	86.91
Day 1	16	11	120	0.1	10	79	85.30
Day 1	17	3	120	1	50	51.6	61.29
Day 1	18	7	60	0.5	30	85	86.91
Day 1	19	3	10	1	10	71	77.77
Day 1	20	11	10	1	10	77	78.43
Day 2	21	7	120	0.5	30	99.1	89.32
Day 2	22	7	60	0.5	10	100	95.18
Day 2	23	11	60	0.5	30	62.7	67.61
Day 2	24	3	60	0.5	30	59.7	57.13
Day 2	25	7	60	0.5	30	88.4	82.66
Day 2	26	7	60	0.1	30	72.1	76.48
Day 2	27	7	60	0.5	30	86.3	82.66
Day 2	28	7	60	0.5	50	70.5	77.67
Day 2	29	7	60	1	30	88	85.96
Day 2	30	7	10	0.5	30	64.9	77.02

**Table 3** The results of analysis of variance (ANOVA)

Source	Sum of squares	Mean square	F-value	p value
Model	5126.88	366.21	5.70	0.0012
A-pH	510.54	510.54	7.95	0.0136
B-Time	705.84	705.84	10.99	0.0051
C-catalyst	420.31	420.31	6.55	0.0227
D-diazinon	1500.20	1500.20	23.36	0.0003
AB	109.20	109.20	1.70	0.2133
AC	28.85	28.85	0.4492	0.5136
AD	17.43	17.43	0.2714	0.6105
BC	16.66	16.66	0.2594	0.6185
BD	9.95	9.95	0.1549	0.6998
CD	119.89	119.89	1.87	0.1934
Lack of fit	889.57	88.96	37.56	0.0016

model’s terms are significant. An *F*-value greater than 0.05, on the other hand, verifies the model’s significance. For the quadratic model, the *p* value is equal to 0.0012, and the *F*-value is equal to 5.70. As a result, the model shows a strong correlation between the actual and predicted values of diazinon removal and is significant at the 95% level.

In order to check the normality of the data, the normal plot residual diagram was used (Fig. 4a). The data are continuous and are plotted on a straight trend line, as can be seen (except for two points). This shows the suitability of the regression model for diazinon photocatalytic degradation. Consequently, the obtained experimental data did not exceed the residual variance (Salarian et al., 2016). On the other hand, the actual and predicted values are very similar, demonstrating the model’s suitability and a strong match, as shown by the predicted versus actual chart (Fig. 4c). The constant variance test was performed using the residual versus predicted graph (Fig. 4b), which also displays the

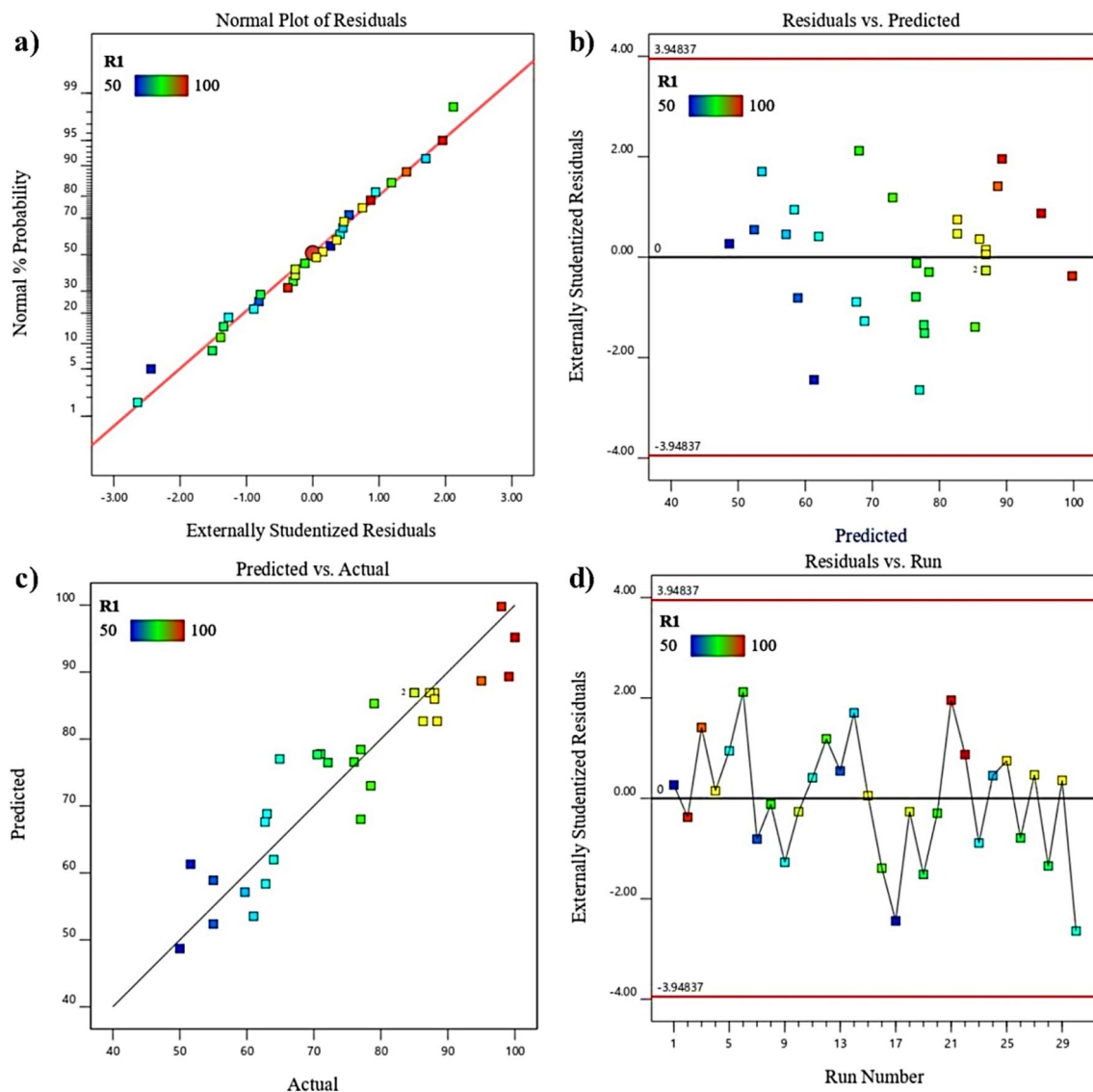


**Fig. 4** **a** Normal plot of residuals, **b** residual versus predicted plot, **c** predicted versus actual plot, **d** residual versus run plot

data's random distribution. As can be seen, the values are distributed randomly and are located between the two red lines. The residual versus run diagram was used to check the data's trend (Fig. 4d). Additionally, this graph showed how random and time-independent the data is. The lack of a trend in this plot indicates that no latent variables were present at the time taken into account that would have affected the response during the experiment (Hu et al., 2021).

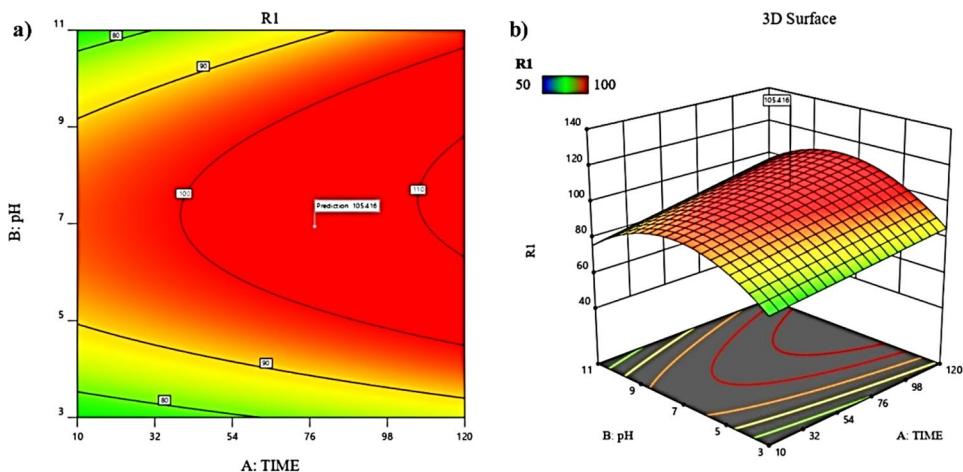
#### Investigating the effect of pH on photodegradation efficiency

One of the most important factors in the photocatalytic degradation of pollutants is pH, which influences the level of ionization, the charge on the surfaces of the pollutants and

oxidants, the number of active species, and the hydrolysis of the pollutants (Mohagheghian et al., 2016). For this purpose, pH was investigated in the range of 3 to 11, and it was observed that the degradation efficiency increases with the increase of pH to 7 and then decreases (Fig. 5). The ZnO/Fe<sub>3</sub>O<sub>4</sub> nanoparticles and diazinon had an excellent electrostatic connection, which is why pH 7 had the maximum degradation efficiency. During the investigation conducted at pHs between 6 and 8, nanoparticles had a positive charge. On the other hand, the pK<sub>a</sub> value of diazinon is 2.6, which has a negative charge at pH higher than 2.6 diazinon (Xu et al., 2021). The highest efficacy of photodegradation is therefore seen at pHs between 6 and 8, where electrostatic attraction is formed. The outcomes are in line with the research by Jonidi-Jafari et al. (2015).



**Fig. 5** Effect of pH on diazinon removal (a 2D diagram, b 3D diagram)



**Investigating the effect of catalytic dose on photodegradation efficiency**

As shown in Fig. 6, the efficiency of photodegradation increases with the amount of ZnO/Fe<sub>3</sub>O<sub>4</sub>, and the maximum amount of diazinon removal is at 1 g/L catalyst. This improvement in efficiency is carried about by an increase in the number of active sites, surface area, and amount of interaction between diazinon and the nanocatalyst. However, it should be noted that increasing the amount of nanocatalyst does not lead to a decrease in removal efficiency. Research has shown that using a lot of nanocatalyst causes turbidity and particle accumulation. This turbidity inhibits light, which decreases the photodegradation efficiency (Sayadi et al., 2022).

**Investigating the effect of diazinon dose on photodegradation efficiency**

The efficacy of photocatalytic degradation was shown to decrease with an increase in diazinon, as shown in Fig. 7. This reduction is due to the occupation of the active sites of the nanoparticles by diazinon particles. The adsorption sites are reduced, and the efficiency of diazinon degradation declines because the number of active species, such as OH, remains unchanged (Chamanepour et al., 2023). Additionally, as the initial materials become more concentrated, the intermediate products that are created compete with them for free radicals, slowing down the rate of degradation. Also, the internal filtering effect, which is caused by a rise

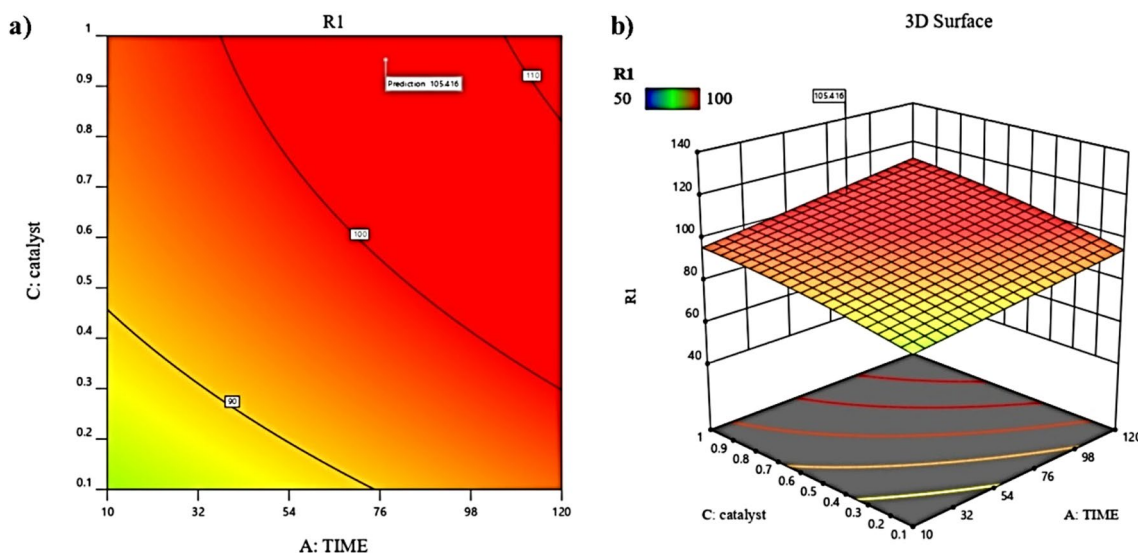


**Fig. 6** Effect of catalyst dose on diazinon removal (a 2D diagram, b 3D diagram)

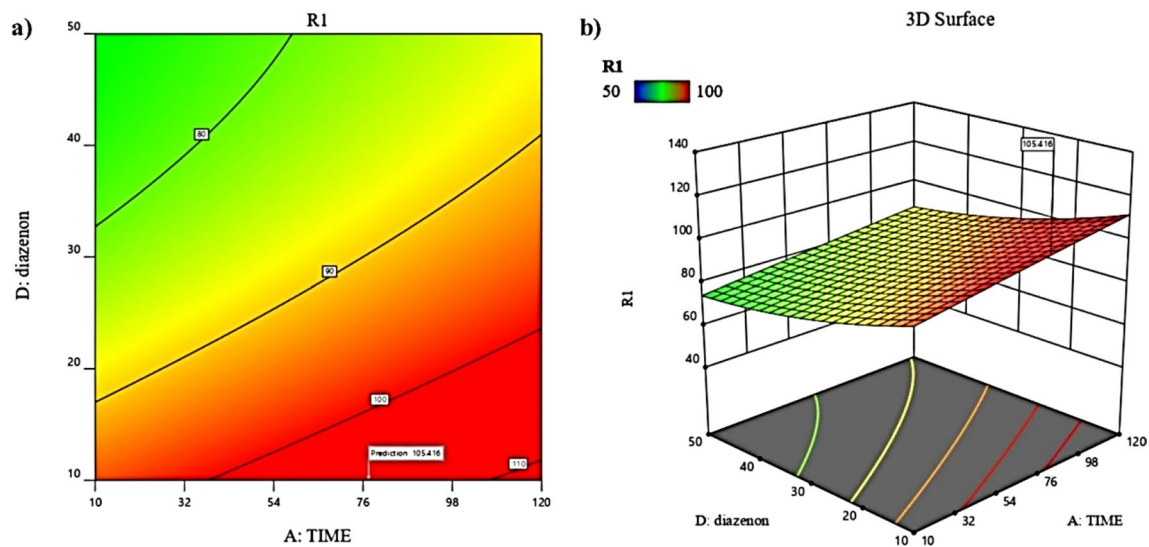


**Fig. 7** Effect of diazinon dose on diazinon removal (a 2D diagram, b 3D diagram)

**Table 4** Optimum conditions for diazinon removal based on BBD model

pH	Time (min)	Catalyst dose (g/L)	Diazinon dose (mg/L)	Removal (%)	Desirability
7	90	1	10	100	1

in diazinon concentration, causes more UV radiation to be absorbed by the diazinon molecules. This action decreases the number of photons that reach the ZnO/Fe<sub>3</sub>O<sub>4</sub> surface (Usman et al., 2017).

#### Investigating the effect of light irradiation on photodegradation efficiency

In the photocatalytic degradation of contaminants, irradiation time is important. The photocatalytic degradation efficiency of diazinon was shown to increase with increasing time, as shown in Figs. 5, 6, and 7. Photocatalyst particles will have additional opportunities to participate in photocatalytic processes by increasing the irradiation time from 10 to 90 min (Molla et al., 2020).

#### Photocatalytic degradation of diazinon under optimal conditions

Finally, the best values for each parameter that maximized the value of diazinon photocatalytic degradation were determined. These values are shown in Table 4. According to the results of the BBD model, time values of 90 min, a nanoparticle concentration of 1 g/L, pH 7, and a diazinon concentration of 10 mg/L were selected as

optimal reaction conditions under which the highest degradation efficiency will be observed. An experiment was carried out in the best possible conditions to verify that the models were satisfactory in predicting the maximal degradation of diazinon. Diazinon's experimental degradation value was 99.3%, which is extremely similar to the amount the BBD model predicted. Also, the amount of photocatalytic degradation of diazinon in optimal conditions for ZnO and Fe<sub>3</sub>O<sub>4</sub> nanoparticles alone was equal to 83.4 and 71.8%, respectively. The results are consistent with other studies. Salarian et al. (2016) found that diazinon's photocatalytic degradation efficiency was 89.21% at optimal conditions of 45 min, 0.1 g/L nanoparticle concentration, and 10 mg/L diazinon concentration. In another study, diazinon poison was broken down by up to 93% in 2 h using a heterogeneous SnS<sub>2</sub>/Bi<sub>4</sub>Ti<sub>3</sub>O<sub>12</sub> photocatalyst (Das et al., 2020).

#### Reuse experiment

The recyclability and durability of the nanoparticles are important parameters that are crucial in practical applications and determine the economy of the nanoparticles. Figure 8 depicts the outcomes of this investigation into the stability of the nanoparticles throughout the duration of five consecutive cycles. The desired nanoparticles were collected with a magnet and then cleaned with distilled water after each photocatalytic experiment. It was then used in a new photocatalytic degradation of diazinon after being dried at 60 °C for 2 h (Chamanehpour et al., 2022). The tests were carried out under optimal conditions of 90 min, 1 g/L nanoparticle concentration, pH 7, and 10 mg/L diazinon concentration. The outcomes demonstrated that

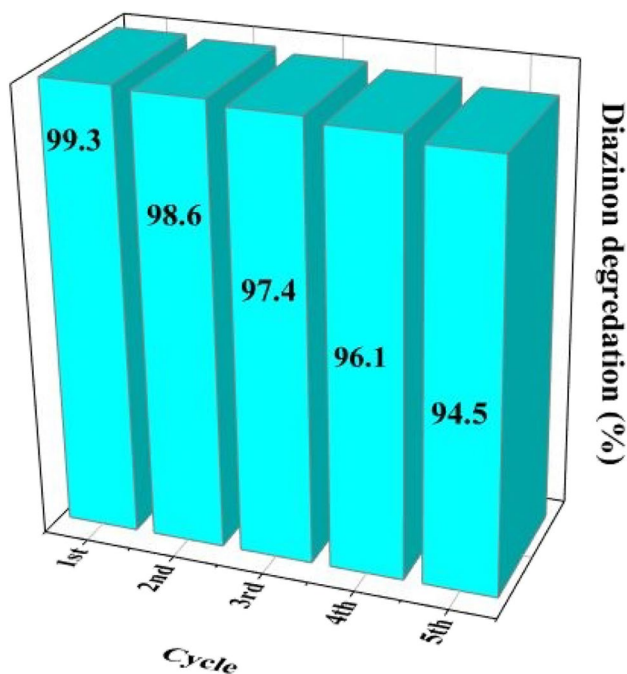


**Fig. 8** Evaluating the efficiency of nanocomposites' reuse activity

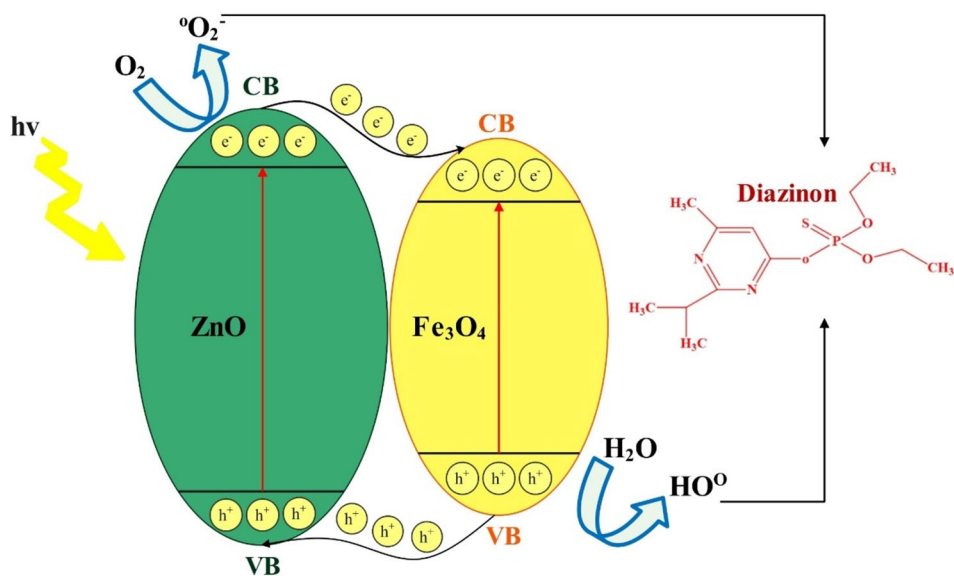
the degrading performance decreased from 99.3 to 94.5% in the last stage of the recycling reaction. ZnO/Fe<sub>3</sub>O<sub>4</sub> nanoparticles, therefore, have a high potential for reuse. This slight decrease can be due to diazinon occluding ZnO/Fe<sub>3</sub>O<sub>4</sub> nanoparticle pores or side product formation, but overall, the produced nanoparticles show acceptable physicochemical stability.

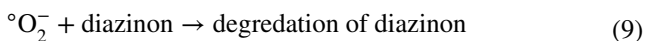
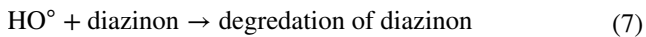
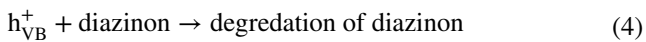
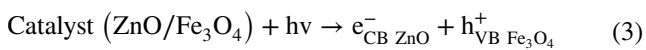
## Degradation mechanism

The mechanism of diazinon toxin degradation by the ZnO/Fe<sub>3</sub>O<sub>4</sub> catalyst is explained based on the photocatalytic process (Fig. 9). The catalyst is stimulated by photon radiation ( $h\nu$ ), which causes the catalyst to create electron-hole pairs on its surface, which then causes the degradation of organic materials. After producing electrons and holes in the photocatalytic process, OH<sup>-</sup> in the aqueous solution is absorbed by valence band holes to produce highly reactive free radicals. Afterward, these free radicals attack the diazinon molecules, which subsequently breakdown into simple products with no destructive effects (Elshypany et al., 2021).

An e<sup>-</sup> is formed in the conduction band of ZnO and a h<sup>+</sup> is formed in the valence band of Fe<sub>3</sub>O<sub>4</sub> by applying ultraviolet radiation ( $h\nu$ ) to the produced nanoparticles (Reaction 3). In fact, photons of light interact with the ZnO/Fe<sub>3</sub>O<sub>4</sub> and transfer energy to the electrons of the catalyst. Then, e<sup>-</sup> moves from CB in ZnO to CB in Fe<sub>3</sub>O<sub>4</sub>, creating a cavity in VB ZnO that may immediately interact with diazinon and cause its destruction (Reaction 4). Additionally, the created hole can react with water to create OH<sup>-</sup> (Reaction 5). Diazinon can be destroyed by the hydroxyl radical created when the generated OH<sup>-</sup> combines with h<sup>+</sup> (Reactions 6 and 7). However, e<sup>-</sup> can also combine with oxygen to form the <sup>o</sup>O<sub>2</sub><sup>-</sup> radical, which has the ability to degrade diazinon (Reactions 8 and 9) (Hassan et al., 2017; Mohammadi et al., 2020). It should be noted that diazinon can break down into byproducts. One of these poisonous substances is known as diazoxon. Additionally, a number of oxygenated side products, including aldehydes, carboxylic acids, and ketones, as well as inorganic ions, like phosphate and ammonium, may be produced. But if complete oxidation takes place, it can be converted into carbon dioxide and water (Jonidi-Jafari et al., 2017).

**Fig. 9** Schematic diagram of diazinon degradation mechanism





## Conclusion

For diazinon photocatalytic degradation, a ZnO/Fe<sub>3</sub>O<sub>4</sub> nanoparticle was used in this study. ZnO and Fe<sub>3</sub>O<sub>4</sub> nanoparticles are well nanoparticles and have a crystalline structure, according to structural analyses and surface morphology. Nanoparticles have an almost spherical and uniform shape, and the average particle size is 41 nm. The ZnO/Fe<sub>3</sub>O<sub>4</sub> nanoparticles display superparamagnetic properties, according to VSM studies. According to the FT-IR data, the synthesized ZnO/Fe<sub>3</sub>O<sub>4</sub> nanoparticle structure contains all functional groups linked to ZnO and Fe<sub>3</sub>O<sub>4</sub>, which can play a key role in pollutant absorption. Also, the XPS results determined the elemental chemical state of the synthesized photocatalyst and the oxidation state of transition metals. According to XPS, the nanoparticle structure contains elements of iron, zinc, carbon, and oxygen. The quadratic model was used for optimization because it also considered the interaction of parameters. The data fit this model at a significance level of 95%. Finally, the results of the photocatalytic experiments demonstrated that the conditions for the highest diazinon removal efficiency were pH 7, a diazinon concentration of 10 mg/L, a nanoparticle concentration of 1 g/L, and a contact time of 90 min. It was observed that with an increase in pH up to 7, the degradation efficiency increases and then decreases. Additionally, the removal efficiency increased with catalyst dosage and contact time, while it decreased with increasing the initial concentration of diazinon. The analyses showed that the photocatalyst's recyclability could increase from 99.3 to 94.5% after 5 recycling cycles, demonstrating the stability and reusability of ZnO/Fe<sub>3</sub>O<sub>4</sub> as a photocatalyst. Therefore, it can be said that the ZnO/Fe<sub>3</sub>O<sub>4</sub> nanoparticles, by producing active free radicals, are able to degrade diazinon, and due to its excellent reusability, ease of separation, and excellent performance in removing diazinon

from aqueous solutions, it can be a cost-effective and promising photocatalyst.

**Author contributions** The paper was conceptualized and supervised by Akram Bemani. The writing was supervised by Akram Bemani and Mohammad Hossein Sayadi. The first and revised draft was prepared by Sima Kalantar and Elham Chamanepour. The investigation, reviewing and editing, methodology, and software were supervised and prepared by Akram Bemani, Mohammad Hossein Sayadi, Elham Chamanepour, and Sima Kalantar.

**Data availability** All data generated or analyzed during this study are included in this published article.

## Declarations

**Ethics approval and consent to participate** Not applicable.

**Consent for publication** Not applicable.

**Competing interests** The authors declare no competing interests.

## References

- Abebe B, Murthy HA, Zerefa E, Adimasu Y (2020a) PVA assisted ZnO based mesoporous ternary metal oxides nanomaterials: synthesis, optimization, and evaluation of antibacterial activity. *Mater Res Exp* 7(4):045011
- Abebe B, Zereffa EA, Murthy HA (2020b) Synthesis of poly (vinyl alcohol)-aided ZnO/Mn<sub>2</sub>O<sub>3</sub> nanocomposites for acid orange-8 dye degradation: mechanism and antibacterial activity. *ACS omega* 6(1):954–964
- Abebe B, Zereffa EA, Murthy HA, Ravikumar CR (2021) A novel poly (vinyl alcohol)-aided ZnO/Fe<sub>2</sub>O<sub>3</sub> nanocomposite as an ascorbic acid sensor. *J Mater Sci Mater Elect* 32:7778–7790
- Ahmadpour N, Sayadi MH, Homaeigohar S (2020) A hierarchical Ca/TiO<sub>2</sub>/NH<sub>2</sub>-MIL-125 nanocomposite photocatalyst for solar visible light induced photodegradation of organic dye pollutants in water. *RSC Adv* 10(50):29808–29820
- Bisht G, Rayamajhi S, Kc B, Paudel SN, Karna D, Shrestha BG (2016) Synthesis, characterization, and study of in vitro cytotoxicity of ZnO-Fe<sub>3</sub>O<sub>4</sub> magnetic composite nanoparticles in human breast cancer cell line (MDA-MB-231) and mouse fibroblast (NIH 3T3). *Nanoscale Res Lett* 11:1–11
- Boruah PK, Das MR (2020) Dual responsive magnetic Fe<sub>3</sub>O<sub>4</sub>-TiO<sub>2</sub>/graphene nanocomposite as an artificial nanozyme for the colorimetric detection and photodegradation of pesticide in an aqueous medium. *J Hazard Mater* 385:121516
- Chamanehpour E, Sayadi MH, Hajjani M (2022) A hierarchical graphitic carbon nitride supported by metal–organic framework and copper nanocomposite as a novel bifunctional catalyst with long-term stability for enhanced carbon dioxide photoreduction under solar light irradiation. *Advanc Comp Hybrid Mater*:1–17
- Chamanehpour E, Sayadi MH, Hajjani M (2023) Metal-organic framework coordinated with g-C<sub>3</sub>N<sub>4</sub> and metal ions for boosting photocatalytic H<sub>2</sub> production under sunlight. *J Photochem Photobiol A: Chemistry* 434:114221
- Chireh M, Naseri M, Ghiasvand S (2019) Enhanced photocatalytic and antibacterial activities of RGO/LiFe<sub>5</sub>O<sub>8</sub> nanocomposites. *J Photochem Photobiol A Chem* 385:112063

- Chu YL, Young SJ, Chu TT, Khosla A, Chiang KY, Ji LW (2021) Improvement of the UV-sensing performance of Ga-doped ZnO nanostructures via a wet chemical solution at room temperature. *ECS J Solid State Sci Technol* 10(12):127001
- Das K, Majhi D, Bariki R, Mishra BG (2020) SnS<sub>2</sub>/Bi<sub>4</sub>Ti<sub>3</sub>O<sub>12</sub> heterostructure material: a UV-visible light active direct Z-scheme photocatalyst for aqueous phase degradation of diazinon. *Chem Select* 5(4):1567–1577
- Dehghani MH, Kamalian S, Shayeghi M, Yousefi M, Heidarinejad Z, Agarwal S, Gupta VK (2019) High-performance removal of diazinon pesticide from water using multi-walled carbon nanotubes. *Microchem J* 145:486–491
- Dehghan S, Kakavandi B, Kalantary RR (2018) Heterogeneous sonocatalytic degradation of amoxicillin using ZnO@Fe<sub>3</sub>O<sub>4</sub> magnetic nanocomposite: influential factors, reusability and mechanisms. *J Mol Liq* 264:98–109
- Długosz O, Szostak K, Krupiński M, Banach M (2021) Synthesis of Fe O /ZnO nanoparticles and their application for the photodegradation of anionic and cationic dyes. *Int J Environ Sci Technol* 18(3):561–574
- Durmus Z, Durmus A, Kavas H (2015) Synthesis and characterization of structural and magnetic properties of graphene/hard ferrite nanocomposites as microwave-absorbing material. *J Mater Sci* 50(3):1201–1213
- Elshypany R, Selim H, Zakaria K, Moustafa AH, Sadeek SA, Sharaa SI et al (2021) Elaboration of Fe<sub>3</sub>O<sub>4</sub>/ZnO nanocomposite with highly performance photocatalytic activity for degradation methylene blue under visible light irradiation. *Environ Technol Inn* 23:101710
- Erim B, Ciğeroğlu Z, Şahin S, Vasseghian Y (2022) Photocatalytic degradation of cefixime in aqueous solutions using functionalized SWCNT/ZnO/Fe<sub>3</sub>O<sub>4</sub> under UV-A irradiation. *Chemosphere* 291:132929
- Farmany A, Mortazavi SS, Mahdavi H (2016) Ultrasound-assisted synthesis of Fe<sub>3</sub>O<sub>4</sub>/SiO<sub>2</sub> core/shell with enhanced adsorption capacity for diazinon removal. *J Magn Magn Mater* 416:75–80
- Ghaderi A, Abbasi S, Farahbod F (2018) Synthesis, characterization and photocatalytic performance of modified ZnO nanoparticles with SnO<sub>2</sub> nanoparticles. *Mater Res Expr* 5(6):065908
- Ghodsi S, Esrafil A, Kalantary RR, Gholami M, Sobhi HR (2020) Synthesis and evaluation of the performance of g-C<sub>3</sub>N<sub>4</sub>/Fe<sub>3</sub>O<sub>4</sub>/Ag photocatalyst for the efficient removal of diazinon: kinetic studies. *J Photochem Photobiol A Chem* 389:112279
- Goyal P, Chakraborty S, Misra SK (2018) Multifunctional Fe<sub>3</sub>O<sub>4</sub>-ZnO nanocomposites for environmental remediation applications. *Environ Nanotechnol, Monit Manag* 10:28–35
- Goyal A, Kapoor S, Samuel P, Kumar V, Singhal S (2015) Facile protocol for reduction of nitroarenes using magnetically recoverable CoM<sub>0.2</sub>Fe<sub>1.8</sub>O<sub>4</sub> (M= Co, Ni, Cu and Zn) ferrite nanocatalysts. *RSC. Advances* 5(63):51347–51363
- Hassan AF, Elhadidy H, Abdel-Mohsen AM (2017) Adsorption and photocatalytic detoxification of diazinon using iron and nanotitania modified activated carbons. *J Taiwan Inst Chem Eng* 75:299–306
- Habibi-Yangjeh A, Golzad-Nonakaran B (2018) Fabrication of magnetically recoverable nanocomposites by combination of Fe<sub>3</sub>O<sub>4</sub>/ZnO with AgI and Ag<sub>2</sub>CO<sub>3</sub>: substantially enhanced photocatalytic activity under visible light. *Phys Chem Res* 6(2):415–431
- Hu YY, Pan C, Zheng X, Hu F, Xu L, Xu G et al (2021) Prediction and optimization of adsorption properties for Cs<sup>+</sup> on NiSiO@NiAlFe LDHs hollow spheres from aqueous solution: kinetics, isotherms, and BBD model. *J Hazard Mater* 401:123374
- Jonidi-Jafari A, Gholami M, Farzadkia M, Esrafil A, Shirzad-Siboni M (2017) Application of Ni-doped ZnO nanorods for degradation of diazinon: kinetics and by-products. *Sep Sci Technol* 52(15):2395–2406
- Jonidi-Jafari A, Shirzad-Siboni M, Yang JK, Naimi-Joubani M, Farrokhi M (2015) Photocatalytic degradation of diazinon with illuminated ZnO–TiO<sub>2</sub> composite. *J Taiwan Inst Chem Eng* 50:100–107
- Kalantary RR, Dadban Shahamat Y, Farzadkia M, Esrafil A, Asghar-nia H (2015) Photocatalytic degradation and mineralization of diazinon in aqueous solution using nano-TiO<sub>2</sub> (Degussa, P25): kinetic and statistical analysis. *Desalin Water Treat* 55(2):555–563
- Liang L, Xi F, Tan W, Meng X, Hu B, Wang X (2021) Review of organic and inorganic pollutants removal by biochar and biochar-based composites. *Biochar* 3(3):255–281
- Liu P, Yao Z, Zhou J (2015) Preparation of reduced graphene oxide/NiO. 4ZnO. 4CoO. 2Fe<sub>2</sub>O<sub>4</sub> nanocomposites and their excellent microwave absorption properties. *Ceram Int* 41(10):13409–13416
- Mahmoodabadi AN, Kompany A, Mashreghi M (2018) Characterization, antibacterial and cytotoxicity studies of graphene-Fe<sub>3</sub>O<sub>4</sub> nanocomposites and Fe<sub>3</sub>O<sub>4</sub> nanoparticles synthesized by a facile solvothermal method. *Mater Chem Phys* 213:285–294
- Molla MAI, Furukawa M, Tateishi I, Katsumata H, Kaneco S (2020) Mineralization of Diazinon with nanosized-photocatalyst TiO<sub>2</sub> in water under sunlight irradiation: optimization of degradation conditions and reaction pathway. *Environ Technol* 41(27):3524–3533
- Mohagheghian A, Karimi SA, Yang JK, Shirzad-Siboni M (2016) Photocatalytic degradation of diazinon by illuminated WO<sub>3</sub> nanopowder. *Desalin Water Treat* 57(18):8262–8269
- Mohammadia M, Malekib A, Zandib S, Mohammadib E, Ghahremanib E, Yangc JK, Leed SM (2020) Photocatalytic decomposition of aqueous diazinon using reduced graphene/ZnO nanocomposite doped with manganese. *Desalin Water Treat* 184:315–325
- Mohammadi M, Maleki A, Zandib S, Mohammadi E, Ghahremani E, Yang JK, Lee SM (2019) Photocatalytic decomposition of aqueous diazinon using reduced graphene/ ZnO nanocomposite doped with manganese. *Desalin Water Treat* 184(2020):315–325
- Naseri M, Naderi E, Sadrolhosseini AR (2016) Effect of phase transformation on physical and biological properties of PVA/CaFe<sub>2</sub>O<sub>4</sub> nanocomposite. *Fibers and Polymers* 17(10):1667–1674
- Polat S, Sayan P (2019) Application of response surface methodology with a Box–Behnken design for struvite precipitation. *Int J Sci Technol Powder Particul Mater*:0921–8831
- Sayadi MH, Ghollasimood S, Ahmadpour N, Homaeigohar S (2022b) Biosynthesis of the ZnO/SnO<sub>2</sub> nanoparticles and characterization of their photocatalytic potential for removal of organic water pollutants. *J Photochem Photobiol A Chem* 425:113662
- Sajjadi S, Khataee A, Bagheri N, Kobya M, Şenocak A, Demirbas E, Karaoğlu AG (2019) Degradation of diazinon pesticide using catalyzed persulfate with Fe<sub>3</sub>O<sub>4</sub>@ MOF-2 nanocomposite under ultrasound irradiation. *J Ind Eng Chem* 77:280–290
- Salarian AA, Hami Z, Mirzaei N, Mohseni SM, Asadi A, Bahrami H et al (2016) N-doped TiO<sub>2</sub> nanosheets for photocatalytic degradation and mineralization of diazinon under simulated solar irradiation: optimization and modeling using a response surface methodology. *J Mol Liq* 220:183–191
- Sayadi MH, Chamanehpour E, Fahoul N (2022a) The ultrasonic process with titanium magnetic oxide nanoparticles to enhance the amoxicillin removal efficiency. *J Water Environ Nanotechnol* 7(3):241–251
- Sayadi MH, Sobhani S, Shekari H (2019) Photocatalytic degradation of azithromycin using GO@ Fe<sub>3</sub>O<sub>4</sub>/ZnO/SnO<sub>2</sub> nanocomposites. *J Clean Prod* 232:127–136
- Sillanpää M, Ncibi MC, Matilainen A, Vepsäläinen M (2018) Removal of natural organic matter in drinking water treatment by coagulation: a comprehensive review. *Chemosphere* 190:54–71
- Sin JC, Tan SQ, Quek JA et al (2018) Facile fabrication of hierarchical porous ZnO/Fe<sub>3</sub>O<sub>4</sub> composites with enhanced magnetic, photocatalytic and antibacterial properties. *Mater Lett* 228:207–211

- Singh TS, Verma TN (2019) Taguchi design approach for extraction of methyl ester from waste cooking oil using synthesized CaO as heterogeneous catalyst: Response surface methodology optimization. *Energy Convers Manag* 182:383–397
- Tabasideh S, Maleki A, Shahmoradi B, Ghahremani E, McKay G (2017) Sonophotocatalytic degradation of diazinon in aqueous solution using iron-doped TiO<sub>2</sub> nanoparticles. *Sep Purif Technol* 189:186–192
- Toolabi A, Malakootian M, Ghaneian MT, Esrafil A, Ehrampoush MH, AskarShahi M, Tabatabaei M (2018) Modeling photocatalytic degradation of diazinon from aqueous solutions and effluent toxicity risk assessment using *Escherichia coli* LMG 15862. *AMB Express* 8(1):1–13
- Usman MR, Noviyanti AR, Eddy DR (2017) Photocatalytic degradation of diazinon using titanium oxide synthesized by alkaline solvent. *Ind J Chem* 17(1):22–29
- Wang J, Yang J, Li X et al (2016) Preparation and photocatalytic properties of magnetically reusable Fe<sub>3</sub>O<sub>4</sub>@ZnO core/shell nanoparticles. *Phys E Low-Dimensional Syst Nanostruct* 75:66–71
- Wang S, Wang X, Qiao G, Chen X, Wang X, Cui H (2021) Core-double shell ZnO@ In<sub>2</sub>O<sub>3</sub>@ ZnO hollow microspheres for superior ethanol gas sensing. *Sensors Actuators B Chem* 341:130002
- Wong YJ, Zhu L, Teo WS, Tan YW, Yang Y, Wang C, Chen H (2011) Revisiting the stober method: inhomogeneity in silica shells. *J Am Chem Soc* 133(30):11422–11425
- Wu H, Li H, Sun G, Ma S, Yang X (2015) Synthesis, characterization and electromagnetic performance of nanocomposites of graphene with  $\alpha$ -LiFeO<sub>2</sub> and  $\beta$ -LiFe<sub>5</sub>O<sub>8</sub>. *J Mater Chem C* 3(21):5457–5466
- Xu X, Meng L, Luo J, Zhang M, Wang Y, Dai Y et al (2021) Self-assembled ultrathin CoO/Bi quantum dots/defective Bi<sub>2</sub>MoO<sub>6</sub> hollow Z-scheme heterojunction for visible light-driven degradation of diazinon in water matrix: intermediate toxicity and photocatalytic mechanism. *Appl Catal B Environ* 293:120231
- Yang H, Ye S, Wang J, Wang H, Wang Z, Chen Q, Tan X (2021) The approaches and prospects for natural organic matter-derived disinfection byproducts control by carbon-based materials in water disinfection progresses. *J Clean Prod* 311:127799
- Zadeh RJ, Sayadi MH, Rezaei MR (2021) Synthesis of thiol modified magMCM-41 nanoparticles with rice husk ash as a robust, high effective, and recycling magnetic sorbent for the removal of herbicides. *J Environ Chem Eng* 9(1):104804
- Zhang L, Wu Y (2013) Sol-gel synthesized magnetic spinel ferrite nanoparticles as novel catalyst for oxidative degradation of methyl orange. *J Nanomater*:2013

**Publisher's note** Springer Nature remains neutral with regard to jurisdictional claims in published maps and institutional affiliations.

Springer Nature or its licensor (e.g. a society or other partner) holds exclusive rights to this article under a publishing agreement with the author(s) or other rightsholder(s); author self-archiving of the accepted manuscript version of this article is solely governed by the terms of such publishing agreement and applicable law.

## Authors and Affiliations

Sima Kalantar<sup>1</sup> · Akram Bemani<sup>1</sup>  · Mohammad Hossein Sayadi<sup>2,3</sup> · Elham Chamanehpour<sup>2</sup>

<sup>1</sup> Department of Environmental Sciences and Engineering, Faculty of Agriculture and Natural Resources, Ardakan University, Ardakan, Iran

<sup>2</sup> Department of Environmental Engineering, Faculty of Natural Resources and Environment, University of Birjand, Birjand, Iran

<sup>3</sup> Department of Agriculture, Faculty of Natural Resources and Environment, Shahid Bahonar University of Kerman, Kerman, Iran